

Application of Neural Ordinary Differential Equations for ITER Burning Plasma Dynamics

Zefang Liu

Fusion Research Center
Georgia Institute of Technology
Atlanta, GA 30332, USA
liuzefang@gatech.edu

Weston M. Stacey

Fusion Research Center
Georgia Institute of Technology
Atlanta, GA 30332, USA
weston.stacey@nre.gatech.edu

Abstract

The dynamics of burning plasmas in tokamaks are crucial for advancing controlled thermonuclear fusion. This study introduces the NeuralPlasmaODE, a multi-region multi-timescale transport model to simulate the complex energy transfer processes in ITER deuterium-tritium (D-T) plasmas. Our model captures the interactions between energetic alpha particles, electrons, and ions, which are vital for understanding phenomena such as thermal runaway instability. We employ neural ordinary differential equations (Neural ODEs) for the numerical derivation of diffusivity parameters, enabling precise modeling of energy interactions between different plasma regions. By leveraging transfer learning, we utilize model parameters derived from DIII-D experimental data, enhancing the efficiency and accuracy of our simulations without training from scratch. Applying this model to ITER's inductive and non-inductive operational scenarios, our results demonstrate that radiation and transport processes effectively remove excess heat from the core plasma, preventing thermal runaway instability. This study underscores the potential of machine learning in advancing our understanding and control of burning plasma dynamics in fusion reactors.

1 Introduction

The dynamics of burning plasmas in tokamaks are critical for advancing controlled thermonuclear fusion. In the International Thermonuclear Experimental Reactor (ITER) [IAEA, 2002], deuterium-tritium (D-T) fusion reactions generate 14.1 MeV neutrons and 3.5 MeV fusion alpha particles [Green et al., 2003]. These alpha particles, confined by magnetic fields, transfer their energy primarily to core electrons before transferring it to ions. The heated core electrons emit various types of radiation, including electron cyclotron radiation (ECR), bremsstrahlung, and impurity radiation, which rapidly dissipate energy compared to the slower transport of energy to the edge. However, the energized electrons and remaining alpha particles also heat the core ions through collisional processes, potentially increasing fusion reactivity and leading to more fusion alpha particles. This positive feedback loop poses a risk of thermal runaway instability in ITER. Consequently, radiation and transport processes between different plasma regions with varying timescales are crucial for effective burning plasma operation.

In previous research [Stacey, 2021, Liu and Stacey, 2021, Liu, 2022, Liu and Stacey, 2024], a multi-region multi-timescale burning plasma dynamics model has been developed to simulate these complex interactions in tokamaks. Different regions, including the core, edge, scrape-off layer (SOL), and divertor, are modeled as separate nodes. This model incorporates essential mechanisms such as auxiliary heating, fusion alpha heating, radiations, collisional energy transfer, transport, and ion orbit loss (IOL). Neural ordinary differential equations (Neural ODEs) [Chen et al., 2018] have

been employed to optimize the parametric diffusivity formula, and this multinodal model has been validated for deuterium plasmas from DIII-D [Liu and Stacey, 2024].

In this study, we extend the multinodal burning plasma dynamics model, NeuralPlasmaODE¹, to analyze ITER D-T plasmas. We make several assumptions suitable for ITER burning plasmas, modeling deuterons, tritons, alpha particles, and electrons in the core and edge nodes. This specialized multinodal model is applied to simulate inductive and non-inductive operational scenarios, examining the dynamics and energy flows among species through various mechanisms with multiple timescales. By leveraging Neural ODEs for the numerical derivation of diffusivity parameters, we enhance the model's precision and efficiency. Additionally, we employ transfer learning to utilize model parameters derived from fitting DIII-D data and avoid the need for training from scratch. The simulation results indicate that radiation and transport processes efficiently remove excess heat from fusion alpha particles, preventing thermal runaway instability. This study highlights the potential of machine learning in improving our understanding and control of burning plasma dynamics in fusion reactors.

2 Burning Plasma Dynamics Model for ITER

To accurately simulate the complex energy transfer processes in ITER burning deuterium-tritium (D-T) plasmas, we develop a multi-region multi-timescale burning plasma dynamics model.

2.1 ITER Plasma Geometry

The geometry of the burning plasma dynamics model is fundamental for simulating ITER plasmas. A conventional tokamak is viewed as a torus with a circular cross-section. The torus is divided into three regions: the core, edge, and scrape-off layer (SOL), following the flux surfaces from the inner to the outer side, while the divertor region is ignored in this geometry. Each region is represented as a separate node in this model, which is illustrated in Appendix A.1 Figure 2.

2.2 Particle and Energy Balance Equations

Based on the assumptions for ITER plasmas in Appendix A.2, the multinodal burning plasma model is presented into the following particle and energy balance equations.

2.2.1 Particle Balance Equations

Particle balance equations for deuterons (D), tritons (T), and alpha particles (α) in the core and edge nodes are

$$\frac{dn_{\sigma}^{\text{core}}}{dt} = S_{\sigma,\text{ext}}^{\text{core}} + S_{\sigma,\text{fus}}^{\text{core}} + S_{\sigma,\text{tran}}^{\text{core}}, \quad (1)$$

$$\frac{dn_{\sigma}^{\text{edge}}}{dt} = S_{\sigma,\text{ext}}^{\text{edge}} + S_{\sigma,\text{fus}}^{\text{edge}} + S_{\sigma,\text{tran}}^{\text{edge}} + S_{\sigma,\text{IOL}}^{\text{edge}}, \quad (2)$$

where $\sigma \in \{D, T, \alpha\}$. The electron densities are computed from the charge neutrality: $n_e^{\text{node}} = z_D n_D^{\text{node}} + z_T n_T^{\text{node}} + z_{\alpha} n_{\alpha}^{\text{node}} + \sum_z z_z n_z^{\text{node}}$, where $\text{node} \in \{\text{core}, \text{edge}\}$ and z is for impurity particles. The particle source and sink terms are discussed in Appendix A.3.1.

2.2.2 Energy Balance Equations

Energy balance equations for deuterons, tritons, alpha particles, and electrons in the core and edge nodes are

$$\frac{dU_{\sigma}^{\text{core}}}{dt} = P_{\sigma,\text{aux}}^{\text{core}} + P_{\sigma,\text{fus}}^{\text{core}} + Q_{\sigma}^{\text{core}} + P_{\sigma,\text{tran}}^{\text{core}}, \quad (3)$$

$$\frac{dU_{\sigma}^{\text{edge}}}{dt} = P_{\sigma,\text{aux}}^{\text{edge}} + P_{\sigma,\text{fus}}^{\text{edge}} + Q_{\sigma}^{\text{edge}} + P_{\sigma,\text{tran}}^{\text{edge}} + P_{\sigma,\text{IOL}}^{\text{edge}}, \quad (4)$$

$$\frac{dU_e^{\text{core}}}{dt} = P_{\Omega}^{\text{core}} + P_{e,\text{aux}}^{\text{core}} + P_{e,\text{fus}}^{\text{core}} - P_R^{\text{core}} + Q_e^{\text{core}} + P_{e,\text{tran}}^{\text{core}}, \quad (5)$$

¹GitHub repository: <https://github.com/zefang-liu/NeuralPlasmaODE>

$$\frac{dU_e^{\text{edge}}}{dt} = P_{\Omega}^{\text{edge}} + P_{e,\text{aux}}^{\text{edge}} + P_{e,\text{fus}}^{\text{edge}} - P_R^{\text{core}} + Q_e^{\text{edge}} + P_{e,\text{tran}}^{\text{edge}}, \quad (6)$$

where $\sigma \in \{D, T, \alpha\}$, the nodal energy density is defined as $U_{\sigma}^{\text{node}} = 3/2 \cdot n_{\sigma}^{\text{node}} T_{\sigma}^{\text{node}}$. The energy source and sink terms are discussed in Appendix A.3.2.

2.3 Diffusivity Models

To compute internodal transport times, it is essential to have formulas for diffusivities. An empirical scaling for the effective thermal diffusivity for ELMy H-mode tokamak plasmas [Becker, 2004] was used as the baseline by Liu and Stacey [2024]. For modeling ITER plasmas accurately, we apply a parametric diffusivity formula for diffusivities [Liu and Stacey, 2024]:

$$\begin{aligned} \frac{\chi(\rho)}{1 \text{ m}^2/\text{s}} = & \alpha_H \left(\frac{B_T}{1 \text{ T}} \right)^{\alpha_B} \left(\frac{n_e(\rho)}{10^{19} \text{ m}^{-3}} \right)^{\alpha_n} \left(\frac{T_e(\rho)}{1 \text{ keV}} \right)^{\alpha_T} \left(\frac{|\nabla T_e(\rho)|}{1 \text{ keV/m}} \right)^{\alpha_{\nabla T}} q(\rho)^{\alpha_q} \kappa(\rho)^{\alpha_{\kappa}} \\ & \cdot \left(\frac{M}{1 \text{ amu}} \right)^{\alpha_M} \left(\frac{R}{1 \text{ m}} \right)^{\alpha_R} \left(\frac{a}{1 \text{ m}} \right)^{\alpha_a}. \end{aligned} \quad (7)$$

where $\alpha_H, \alpha_B, \dots, \alpha_a$ are parameters to be determined and all physical values are listed in Appendix A.4. This diffusivity formula can be expressed in vector form as $\ln \chi_{\text{node}} = \mathbf{b}_{\text{node}} + \mathbf{W}_{\text{node}} \ln \mathbf{x}_{\text{node}}$, where χ_{node} represents the internodal diffusivities vector, \mathbf{b}_{node} is the bias vector, \mathbf{W}_{node} is the weight matrix, and \mathbf{x}_{node} is the vector of corresponding physical values.

3 Simulations for ITER Plasmas

In this section, we present our simulations for ITER plasmas, including introducing the various simulation scenarios, discussing the simulation methodology, and analyzing the simulation results.

3.1 Simulation Scenarios

The multinodal burning plasma dynamics model is applied to simulate the ITER deuterium-tritium (D-T) plasma. The ITER heating and current drive (H&CD) system [IAEA, 2002, Shimada et al., 2007, Henderson et al., 2015] includes neutral beam injection (NB), ion cyclotron heating (IC), electron cyclotron heating (EC), and lower hybrid heating (LH). The ITER tokamak can operate in both inductive and non-inductive modes. In the inductive mode, the ohmic current is the primary contributor to the total toroidal current, while in the non-inductive mode, highly energetic neutral atom injection and powerful radiofrequency radiation drive most of the toroidal current. For this study, we select inductive scenario 2, hybrid scenario 3, and non-inductive scenario 4 from the ITER design [IAEA, 2002]. Their typical operating conditions are exhibited in Appendix C.1.

3.2 Simulation Methodology

To accurately model the ITER burning plasma, the parameters in the diffusivity model need to be properly tuned using machine learning. The computational framework based on neural ordinary differential equations (Neural ODEs) [Chen et al., 2018], NeuralPlasmaODE, is presented in Appendix B. In the previous study on simulating DIII-D plasmas with NeuralPlasmaODE, Liu and Stacey [2024] split experimental data into training and testing datasets. The training dataset was used to tune parameters in the diffusivity model, while the testing dataset evaluated the optimized model. However, since the ITER is still under construction and its experimental data are unavailable, we adopt transfer learning [Weiss et al., 2016], where the diffusivity parameters learned from DIII-D deuterium plasmas are transferred to ITER plasmas. We then apply a fine-tuning method to these diffusivity parameters using burning simulation results from prior research [IAEA, 2002, Green et al., 2003] as optimization targets. The parameters in the diffusivity model are adjusted to match the ITER design scenarios during the current flat-top phase.

The optimization objective is defined as a vector including densities and temperatures in the core and edge nodes:

$$\left[n_D^{\text{node}}/10^{19} \text{ m}^{-3} \quad n_{\alpha}^{\text{node}}/10^{18} \text{ m}^{-3} \quad n_e^{\text{node}}/10^{19} \text{ m}^{-3} \quad T_D^{\text{node}}/1 \text{ keV} \quad T_e^{\text{node}}/1 \text{ keV} \right], \quad (8)$$

with the nodal diffusivity parameters initialized to those of the DIII-D plasma. Densities and temperatures are initialized at current flat-top values instead of a cold plasma, with a time step of 0.2 s and a total simulation time of 10 s. After 14 epochs, the mean squared error (MSE) loss for scenario 2 in the current flat-top phase drops from 6.7085 to 0.0016 with a learning rate of 0.02. The optimized multinodal model is then used to simulate both inductive and hybrid scenarios. For non-inductive scenarios, diffusivity parameters are transferred from inductive scenarios and trained on scenario 4 with 2 epochs and a learning rate of 0.02, reducing the MSE loss from 13.2741 to 0.6333. After the optimization, initial temperatures are reset to 2 keV in the core node and 1 keV in the edge node for all species, with particle densities from Appendix C.1, except alpha particle densities set to 10^{17} m^{-3} . The multinodal model is then simulated for ITER scenarios over a total time of 15 s.

3.3 Simulation Results

The inductive scenario represents a mode of operation where the majority of the plasma current is driven by ohmic heating and auxiliary heating systems. The simulation results for inductive scenario 2 are presented in Figure 1, showing the densities and temperatures of deuterons, alpha particles, and electrons. Triton densities and temperatures are omitted as they are approximately the same as those of deuterons. Additionally, the temperatures of alpha particles are shown only for the cold ones, excluding fusion alpha particles at 3.5 MeV until they transfer their energy to electrons and ions. The results indicate that core and edge temperatures reach a steady state at around 11 s, and no energy excursion due to fusion alpha heating is observed. Furthermore, Figure 5 in Appendix C.2 depicts the power changes over time.

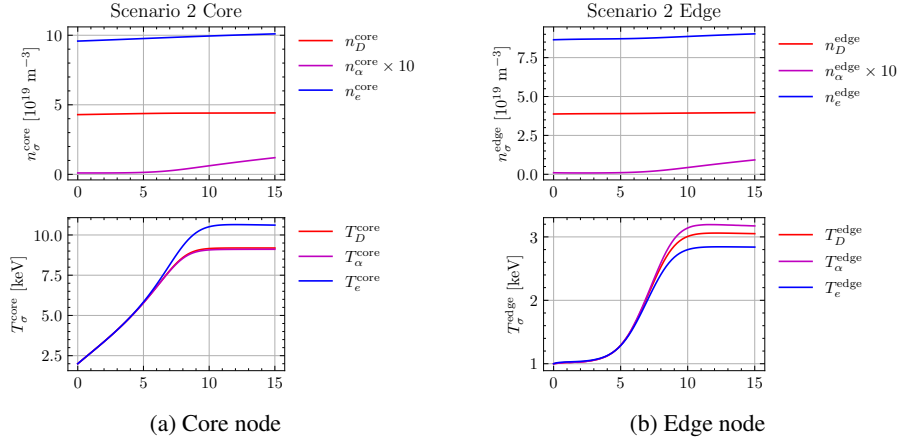


Figure 1: Densities and temperatures of ITER inductive operation scenario 2.

Simulations results and analyses for hybrid and non-inductive operation scenarios are presented in Appendix C.3 and C.4.

4 Conclusion

In this research, we simulate ITER deuterium-tritium (D-T) plasmas using NeuralPlasmaODE, a multi-region multi-timescale transport model, to understand complex energy transfer processes. By employing neural ordinary differential equations (Neural ODEs) and leveraging transfer learning with parameters derived from DIII-D experimental data, we enhance simulation efficiency and accuracy. The model is applied to both inductive and non-inductive operational scenarios of ITER, showing that in inductive scenarios, core electrons dissipate energy through various radiation mechanisms, while in non-inductive scenarios, most plasma current is generated non-inductively, leading to higher core temperatures and significant energy transport to the edge. In both scenarios, radiation and transport processes effectively prevent thermal runaway instability, highlighting the potential of machine learning to advance our understanding and control of burning plasma dynamics in fusion reactors.

References

- F Albajar, J Johner, and G Granata. Improved calculation of synchrotron radiation losses in realistic tokamak plasmas. *Nuclear fusion*, 41(6):665, 2001.
- Ferran Albajar, Marino Bornatici, and Folker Engelmann. Raytec: a new code for electron cyclotron radiative transport modelling of fusion plasmas. *Nuclear Fusion*, 49(11):115017, 2009.
- G Becker. Study of anomalous inward drift in tokamaks by transport analysis and simulations. *Nuclear fusion*, 44(9):933, 2004.
- G Becker and O Kardaun. Anomalous particle pinch and scaling of vin/d based on transport analysis and multiple regression. *Nuclear fusion*, 47(1):33, 2006.
- H-S Bosch and Gerald M Hale. Improved formulas for fusion cross-sections and thermal reactivities. *Nuclear fusion*, 32(4):611, 1992.
- Ricky TQ Chen, Yulia Rubanova, Jesse Bettencourt, and David K Duvenaud. Neural ordinary differential equations. *Advances in neural information processing systems*, 31, 2018.
- BJ Green et al. Iter: burning plasma physics experiment. *Plasma physics and controlled fusion*, 45(5):687, 2003.
- M Henderson, G Saibene, C Darbos, D Farina, L Figini, M Gagliardi, F Gandini, T Gassmann, G Hanson, A Loarte, et al. The targeted heating and current drive applications for the iter electron cyclotron system. *Physics of plasmas*, 22(2), 2015.
- IAEA. *ITER Technical Basis*. Number 24 in ITER EDA Documentation Series. International Atomic Energy Agency, Vienna, 2002.
- CE Kessel, G Giruzzi, ACC Sips, RV Budny, JF Artaud, V Basiuk, F Imbeaux, E Joffrin, M Schneider, M Murakami, et al. Simulation of the hybrid and steady state advanced operating modes in iter. *Nuclear Fusion*, 47(9):1274, 2007.
- Zefang Liu. *A Multi-Region Multi-Timescale Burning Plasma Dynamics Model for Tokamaks*. PhD thesis, Georgia Institute of Technology, 2022.
- Zefang Liu and Weston Stacey. A multi-region multi-timescale burning plasma dynamics model for tokamaks. In *APS Division of Plasma Physics Meeting Abstracts*, volume 2021, pages UP11–087, 2021.
- Zefang Liu and Weston M Stacey. Application of neural ordinary differential equations for tokamak plasma dynamics analysis. *arXiv preprint arXiv:2403.01635*, 2024.
- D Kh Morozov, EO Baronova, and I Yu Senichenkov. Impurity radiation from a tokamak plasma. *Plasma Physics Reports*, 33:906–922, 2007.
- DE Roberts. Total impurity radiation power losses from steady-state tokamak plasmas. *Nuclear Fusion*, 21(2):215, 1981.
- M Shimada, DJ Campbell, V Mukhovatov, M Fujiwara, N Kirneva, K Lackner, M Nagami, VD Pustovitov, N Uckan, J Wesley, et al. Overview and summary. *Nuclear Fusion*, 47(6):S1, 2007.
- Weston M Stacey. The effect of ion orbit loss and x-loss on the interpretation of ion energy and particle transport in the diii-d edge plasma. *Physics of Plasmas*, 18(10), 2011.
- Weston M Stacey. *Fusion plasma physics*. John Wiley & Sons, 2012.
- Weston M Stacey. Effect of ion orbit loss on distribution of particle, energy and momentum sources into the tokamak scrape-off layer. *Nuclear Fusion*, 53(6):063011, 2013.
- Weston M Stacey. A nodal model for tokamak burning plasma space-time dynamics. *Fusion Science and Technology*, 77(2):109–118, 2021.

- Weston M Stacey and Matthew T Schumann. The distribution of ion orbit loss fluxes of ions and energy from the plasma edge across the last closed flux surface into the scrape-off layer. *Physics of Plasmas*, 22(4), 2015.
- F Wagner, A Becoulet, R Budny, V Erckmann, D Farina, G Giruzzi, Y Kamada, A Kaye, F Koechl, K Lackner, et al. On the heating mix of iter. *Plasma Physics and Controlled Fusion*, 52(12): 124044, 2010.
- Karl Weiss, Taghi M Khoshgoftaar, and DingDing Wang. A survey of transfer learning. *Journal of Big data*, 3:1–40, 2016.
- John Wesson and David J Campbell. *Tokamaks*, volume 149. Oxford university press, 2011.
- TM Wilks and WM Stacey. Improvements to an ion orbit loss calculation in the tokamak edge. *Physics of Plasmas*, 23(12), 2016.

A Burning Plasma Dynamics Model Details

A.1 ITER Plasma Geometry Illustrations

The burning plasma dynamics model represents the ITER plasma as a toroidal tokamak geometry, divided into core, edge, and scrape-off layer (SOL) regions as separate nodes, as shown in Figure 2. In this model, each node is a toroidal shell with interfaces represented as torus surfaces. The minor radii for the surfaces r_{core} , r_{edge} , and r_{sol} correspond to the core, edge, and SOL surfaces respectively. The radial distances between these nodes are defined as $\Delta r_{\text{core-edge}}$ for the core to edge, $\Delta r_{\text{edge-sol}}$ for the edge to SOL, and $\Delta r_{\text{sol-div}}$ for the distance from the SOL node center to its outer surface. These radial distances are calculated as $\Delta r_{\text{core-edge}} = r_{\text{edge}}/2$, $\Delta r_{\text{edge-sol}} = (r_{\text{sol}} - r_{\text{core}})/2$, and $\Delta r_{\text{sol-div}} = (r_{\text{sol}} - r_{\text{edge}})/2$. Additionally, the normalized minor radius is defined as $\rho = r/a$, where a is the minor radius of the plasma.

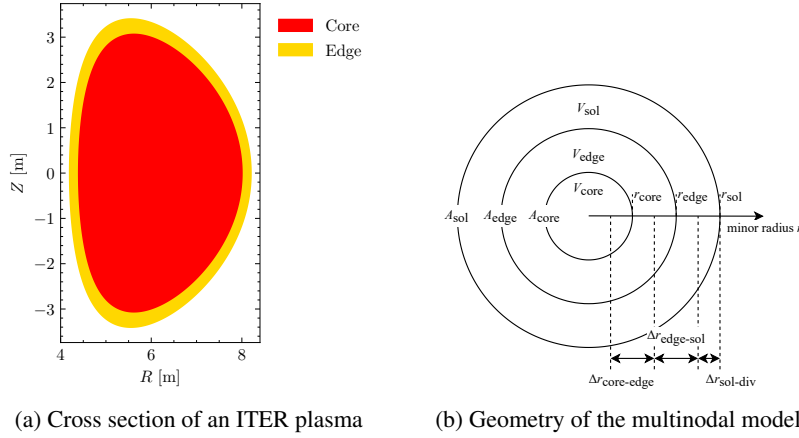


Figure 2: Multinodal model geometry of tokamak plasmas, where the left figure shows the cross section of an ITER plasma, and the right figure is the simplified geometry in the multinodal model.

A.2 Assumptions for ITER Plasmas

To simulate ITER D-T plasmas, the multinodal burning plasma model [Liu and Stacey, 2024] requires several necessary modifications to balance accuracy and computational efficiency. 1) Only the core and edge regions are modeled as separate nodes. 2) The model computes the behavior of deuterons, tritons, alpha particles, and electrons, while including helium, beryllium, and argon as impurity particles. 3) The simulation focuses solely on the D-T fusion reaction, while all atomic and molecular processes, as well as neutral and recycling particles, are neglected. 4) The triton particle and thermal diffusivities are assumed to be equal to those of deuterons. 5) A delay mechanism for fusion alpha heating is implemented in the core node. 6) Predetermined energy deposition profiles for neutral beam injection (NBI) and radiofrequency (RF) heating [Kessel et al., 2007] are utilized. 7) Electron cyclotron radiation (ECR) [Albajar et al., 2001, 2009] parameters, fitted for typical ITER profiles, are applied. 8) Ion orbit loss (IOL) [Stacey, 2011, 2013, Wilks and Stacey, 2016] is considered only for the edge node, with approximated loss timescales equated to transport times.

A.3 Physical Terms in Particle and Energy Balance Equations

We enumerate the physical terms used for the particle and energy balance equations in Section 2.2 as follows.

A.3.1 Physical Terms in Particle Balance Equations

The **external particle sources** are computed by summing the neutral beam injection (NBI), gas puffing (GAS), shatter pellet injection (SPI), and other external particle sources: $S_{\sigma, \text{ext}}^{\text{node}} = S_{\sigma, \text{NBI}}^{\text{node}} + S_{\sigma, \text{GAS}}^{\text{node}} + S_{\sigma, \text{SPI}}^{\text{node}} + \dots$, where $\sigma \in \{D, T, \alpha\}$. In this research, only particle sources from the NBI [Wesson and Campbell, 2011] are considered. The **fusion terms** are computed from the D-T fusion

reactions [Stacey, 2012] by $S_{D,\text{fus}}^{\text{node}} = S_{T,\text{fus}}^{\text{node}} = -n_D^{\text{node}} n_T^{\text{node}} \langle \sigma v \rangle_{\text{fus}}$ and $S_{\alpha,\text{fus}}^{\text{node}} = n_D^{\text{node}} n_T^{\text{node}} \langle \sigma v \rangle_{\text{fus}}$, where $\langle \sigma v \rangle_{\text{fus}}$ is the fusion reactivity [Bosch and Hale, 1992]. The **particle transport terms** in the core and edge nodes are computed by $S_{\sigma,\text{tran}}^{\text{core}} = -(n_\sigma^{\text{core}} - n_\sigma^{\text{edge}})/\tau_{P,\sigma}^{\text{core} \rightarrow \text{edge}}$ and $S_{\sigma,\text{tran}}^{\text{edge}} = V_{\text{core}}/V_{\text{edge}} \cdot (n_\sigma^{\text{core}} - n_\sigma^{\text{edge}})/\tau_{P,\sigma}^{\text{core} \rightarrow \text{edge}} - n_\sigma^{\text{edge}}/\tau_{P,\sigma}^{\text{edge} \rightarrow \text{sol}}$, where $\tau_{P,\sigma}^{\text{core} \rightarrow \text{edge}}$ (or $\tau_{P,\sigma}^{\text{edge} \rightarrow \text{sol}}$) is the particle transport time from the core (or edge) node to the edge (or SOL) node. These particle transport times [Liu, 2022] are calculated by $\tau_{P,\sigma}^{\text{core} \rightarrow \text{edge}} = (r_{\text{core}}^2 \Delta r_{\text{core-edge}})/(2r_{\text{core}} D_\sigma^{\text{core}})$ and $\tau_{P,\sigma}^{\text{edge} \rightarrow \text{sol}} = ((r_{\text{edge}}^2 - r_{\text{core}}^2) \Delta r_{\text{edge-sol}})/(2r_{\text{edge}} D_\sigma^{\text{edge}})$, where D_σ^{core} and D_σ^{edge} are the core and edge particle diffusivities respectively. The **ion orbit loss (IOL) terms** are computed by $S_{\sigma,\text{IOL}}^{\text{edge}} = -F_{\sigma,\text{orb}}^{\text{edge}}/\tau_{P,\sigma,\text{IOL}}^{\text{edge}} \cdot n_\sigma^{\text{edge}}$, where $F_{\sigma,\text{orb}}^{\text{edge}}$ is the particle loss fraction [Stacey, 2011, Stacey and Schumann, 2015], and $\tau_{P,\sigma,\text{IOL}}^{\text{edge}}$ is the particle IOL timescale.

A.3.2 Physical Terms in Energy Balance Equations

The **ohmic heating power** [Stacey, 2012] is computed from the plasma current I_P by $P_\Omega^{\text{node}} (\text{W/m}^3) = 2.8 \times 10^{-9} (Z_{\text{eff}} I_P^2)/(a^4 T_e^{3/2})$. The **auxiliary heating terms** contain the neutral beam injection (NBI) and radiofrequency (RF) heating (including ion cyclotron heating (ICH), electron cyclotron heating (ECH), and lower hybrid heating (LH)): $P_{i,\text{aux}}^{\text{node}} = P_{i,\text{NBI}}^{\text{node}} + P_{i,\text{ICH}}^{\text{node}}$ and $P_{e,\text{aux}}^{\text{node}} = P_{e,\text{NBI}}^{\text{node}} + P_{e,\text{ECH}}^{\text{node}} + P_{e,\text{LH}}^{\text{node}}$. The **fusion power** is $P_{\sigma,\text{fus}}^{\text{node}} = n_D^{\text{node}} n_T^{\text{node}} \langle \sigma v \rangle_{\text{fus}} U_{f\sigma}$, where $\sigma \in \{D, T, \alpha\}$ and $U_{f\sigma}$ is the fusion energy transferred to the species σ calculated by NBI heating formulas [Wesson and Campbell, 2011]. The delay effect between fusion alpha heating to electrons and ions is considered by a slowing-down timescale τ_{se}^{node} as $\tau_{se} = (3\sqrt{2}\pi T_e^{3/2})/(m_e^{1/2} m_b A_D)$. The fusion reaction rate $S_{\text{fus}}^{\text{node}}$ for core ions is evaluated at $T_i^{\text{node}}(t - \tau_{se}) \approx T_i^{\text{node}}(t) - dT_i^{\text{node}}/dt(t) \cdot \tau_{se}$, so the fusion heating to ions is postponed by this timescale compared with electrons. **Collisional energies** transferred between ions and electrons are $Q_\alpha^{\text{node}} = Q_{\alpha D}^{\text{node}} + Q_{\alpha T}^{\text{node}} + Q_{\alpha e}^{\text{node}}$, $Q_e^{\text{node}} = -Q_{\alpha e}^{\text{node}} - Q_{De}^{\text{node}} - Q_{Te}^{\text{node}}$, $Q_D^{\text{node}} = -Q_{\alpha D}^{\text{node}} + Q_{DT}^{\text{node}} + Q_{De}^{\text{node}}$, and $Q_T^{\text{node}} = -Q_{\alpha T}^{\text{node}} - Q_{DT}^{\text{node}} + Q_{Te}^{\text{node}}$, where $Q_{\sigma\sigma'}$ is the energy transferred from the species σ' to σ [Stacey, 2012]. The **radiation terms** from electron cyclotron radiation (ECR) [Albajar et al., 2001], bremsstrahlung [Stacey, 2012], and impurity radiation [Stacey, 2012, Roberts, 1981, Morozov et al., 2007] are computed by $P_R^{\text{node}} = P_{\text{ECR}}^{\text{node}} + P_{\text{brem}}^{\text{node}} + P_{\text{imp}}^{\text{node}}$. The **energy transport terms** in the core and edge nodes are $P_{\sigma,\text{tran}}^{\text{core}} = -(U_\sigma^{\text{core}} - U_\sigma^{\text{edge}})/\tau_{E,\sigma}^{\text{core} \rightarrow \text{edge}}$ and $P_{\sigma,\text{tran}}^{\text{edge}} = V_{\text{core}}/V_{\text{edge}} \cdot (U_\sigma^{\text{core}} - U_\sigma^{\text{edge}})/\tau_{E,\sigma}^{\text{core} \rightarrow \text{edge}} - U_\sigma^{\text{edge}}/\tau_{E,\sigma}^{\text{edge} \rightarrow \text{sol}}$, where $\tau_{E,\sigma}^{\text{core} \rightarrow \text{edge}}$ (or $\tau_{E,\sigma}^{\text{edge} \rightarrow \text{sol}}$) is the energy transport time from the core (or edge) node to the edge (or SOL) node. These energy transport times [Liu, 2022] are solved from $\tau_{E,\sigma}^{\text{core} \rightarrow \text{edge}} = (r_{\text{core}}^2 \Delta r_{\text{core-edge}})/(2r_{\text{core}} \chi_\sigma^{\text{core}})$ and $\tau_{E,\sigma}^{\text{edge} \rightarrow \text{sol}} = ((r_{\text{edge}}^2 - r_{\text{core}}^2) \Delta r_{\text{edge-sol}})/(2r_{\text{edge}} \chi_\sigma^{\text{edge}})$, where $\chi_\sigma^{\text{core}}$ and $\chi_\sigma^{\text{edge}}$ are the core and edge thermal diffusivities respectively. The **IOL terms** for the edge node are computed by $P_{D,\text{IOL}}^{\text{edge}} = -E_{D,\text{orb}}^{\text{edge}}/\tau_{E,D,\text{IOL}}^{\text{edge}} \cdot U_D^{\text{edge}}$, where $E_{D,\text{orb}}^{\text{edge}}$ is the energy loss fraction [Stacey, 2011, Stacey and Schumann, 2015], and $\tau_{E,D,\text{IOL}}^{\text{edge}}$ is the energy IOL timescale.

A.4 More Diffusivity Models

An empirical scaling for the effective thermal diffusivity in ELMy H-mode tokamak plasmas [Becker, 2004] is given by:

$$\chi_{H98}(\rho) = \alpha_H B_T^{-3.5} n_e(\rho)^{0.9} T_e(\rho) |\nabla T_e(\rho)|^{1.2} q(\rho)^{3.0} \kappa(\rho)^{-2.9} M^{-0.6} R^{0.7} a^{-0.2} (\text{m}^2/\text{s}), \quad (9)$$

where the thermal diffusivity χ_{H98} in m^2/s , normalized radius $\rho = r/a$, coefficient $\alpha_H = 0.123$, toroidal magnetic field B_T in T, electron density n_e in 10^{19}m^{-3} , electron temperature T_e in keV, electron temperature gradient ∇T_e in keV/m, safety factor $q = q_\psi$, local elongation κ , hydrogenic atomic mass number M in 1 amu, major radius R in m, and minor radius a in m. The particle and thermal diffusivities for electrons and ions [Becker and Kardaun, 2006] can be assumed as $\chi_e(\rho) = \chi_i(\rho) = \chi_{H98}(\rho)$ and $D_i(\rho) = 0.6\chi_{H98}(\rho)$.

B Computational Framework of NeuralPlasmaODE

In this study, we enhance the computational framework of NeuralPlasmaODE from Liu and Stacey [2024] to simulate burning plasma dynamics in ITER. Figure 3 shows a workflow diagram of it. This

framework consists of several modules designed for processing experimental data, simulating plasma behavior, and optimizing model parameters. The burning plasma dynamics is solved using the neural ordinary differential equation (Neural ODE) [Chen et al., 2018] solver.

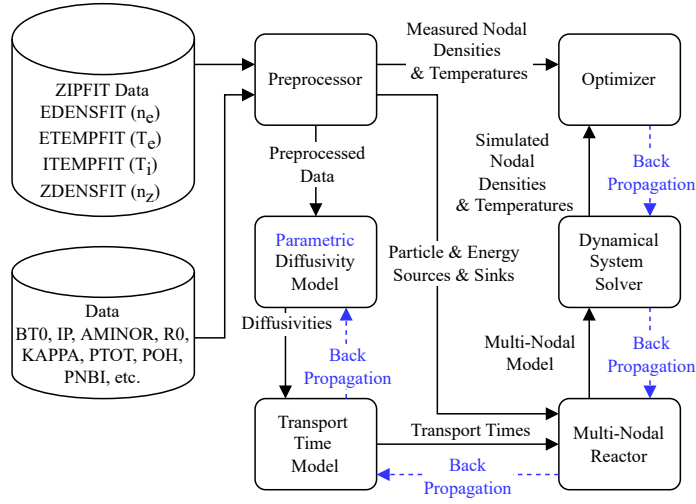


Figure 3: Computational framework of NeuralPlasmaODE, including cylinders as datasets, squares as modules, solid lines as forward flows, and dashed lines as back propagation processes.

C Simulation Details

C.1 Simulation Scenario Parameters

Typical parameters of ITER inductive, hybrid, and non-inductive operation scenarios [IAEA, 2002] are presented in Table 1. The important parameters are contained, including geometries, electromagnetic values, auxiliary heating powers, densities, temperatures, and impurity fractions. Moreover, the typical radial profiles of electron and ion temperatures, and electron and helium densities are depicted in Figure 4.

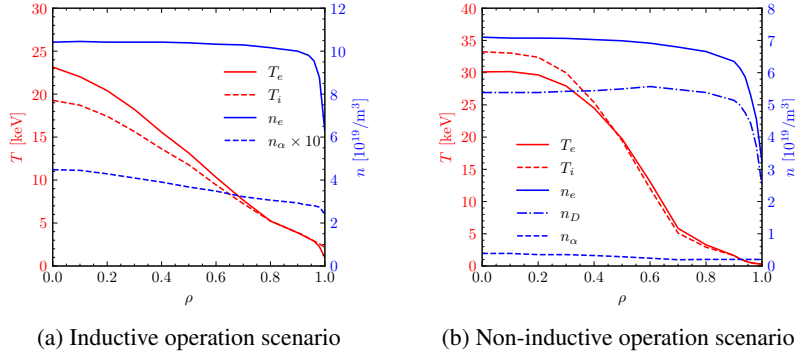


Figure 4: Typical radial profiles of plasma temperatures and densities in the ITER inductive and non-inductive operation scenarios (reproduced with permission from IAEA [2002]).

For simulating the ITER design scenarios, we model several essential particle and energy sources. For external particle sources, neutral beam injection introduces negative deuteron particles into the tokamak plasma, with an equal amount of tritons assumed to be supplied to maintain a balance between deuteron and triton particles. For external energy sources, neutral beam and radiofrequency (RF) heating systems provide auxiliary heating. In the inductively driven scenario, Wagner et al. [2010] concluded that the exact proportions of NB, IC, and EC heating are not critical, but IC heating should be utilized to heat ions directly. Therefore, we assume all RF heating power is deposited into ions in this scenario.

Table 1: Typical parameters of inductive, hybrid, and non-inductive ITER operation scenarios (reproduced with permission from IAEA [2002]).

Parameter	Symbol	Inductive Scenario 2	Hybrid Scenario 3	Non-Inductive Scenario 4
Major radius	R_0 (m)	6.2	6.2	6.35
Minor radius	a (m)	2.0	2.0	1.85
Volume	V (m ³)	831	831	794
Surface	S (m ²)	683	683	-
Elongation at the 95% flux surface	κ_{95}	1.70	1.70	1.85
Triangularity at the 95% flux surface	δ_{95}	0.33	0.33	0.40
Toroidal magnetic field at the magnetic axis	B_T (T)	5.3	5.3	5.18
Plasma current	I_P (MA)	15	13.8	9.0
Safety factor at the 95% flux surface	q_{95}	3.0	3.3	5.3
Volume-averaged electron density	$\langle n_e \rangle$ (10 ¹⁹ m ⁻³)	10.1	9.3	6.7
Volume-averaged ion temperature	$\langle T_i \rangle$ (keV)	8.0	8.4	12.5
Volume-averaged electron temperature	$\langle T_e \rangle$ (keV)	8.8	9.6	12.3
Fusion power	P_{fus} (MW)	400	400	356
Auxiliary heating power	P_{aux} (MW)	40	73	59
Radiofrequency heating power	P_{RF} (MW)	7	40	-
Lower hybrid heating power	P_{LH} (MW)	-	-	29
Neutral beam heating power	P_{NBI} (MW)	33	33	30
Fusion energy gain factor	Q	10	5.4	6.0
Energy confinement time	τ_E (s)	3.7	2.73	3.1
Burn time	t (s)	400	1070	3000
Helium fraction	f_{He} (%)	3.2	2.5	4.1
Beryllium fraction	f_{Be} (%)	2.0	2.0	2.0
Argon fraction	f_{Ar} (%)	0.12	0.19	0.26
Effective impurity charge	Z_{eff}	1.66	1.85	2.07
Radiation power	P_{rad} (MW)	47	55	37.6

C.2 Inductive Operation Scenario Results

Figure 5 depicts the power changes over time, with positive values indicating energy gain and negative values indicating energy loss. At the start of the simulation, ohmic heating (P_{oh}^{core}) and auxiliary heating ($P_{\sigma,aux}^{core}$) provide most of the energy to core electrons and ions until the core ion temperature becomes high enough to initiate fusion reactions. Fusion alpha particles first heat the electrons ($P_{e,fus}^{core}$), after which the heated electrons transfer their energy to ions through Coulomb collisions ($Q_i^{core} = -Q_e^{core}$). Meanwhile, fusion heating is also deposited directly to core ions ($P_{i,fus}^{core}$). The fusion heating is then removed by radiation power (P_{rad}^{core}) and transport loss ($P_{\sigma,tran}^{core}$).

C.3 Hybrid Operation Scenario Results

A hybrid mode of operation, where a significant fraction of the plasma current is driven by non-inductive current drive power and the bootstrap current, is a promising route for establishing steady-state or non-inductive modes in ITER [IAEA, 2002]. To verify thermal stability with fusion alpha heating, we selected scenario 3 for simulation using the multinodal burning plasma dynamics model. The results for this scenario are shown in Figures 6 and 7, first displaying the densities and temperatures, followed by the power profiles. The ion and electron temperatures reach a steady state at around 6 s, which is shorter than in the inductive scenarios due to the higher auxiliary heating power. This increased auxiliary heating is offset by higher radiation and transport losses, preventing any power excursion in this hybrid scenario simulation.

C.4 Non-Inductive Operation Scenario Results

The non-inductive operation scenario selected for this study is weak negative shear (WNS) scenario 4. Compared to the inductive profiles, the typical radial profiles in Figure 4 show a higher core temperature with a steeper temperature gradient. The plasma current in the non-inductive scenario is

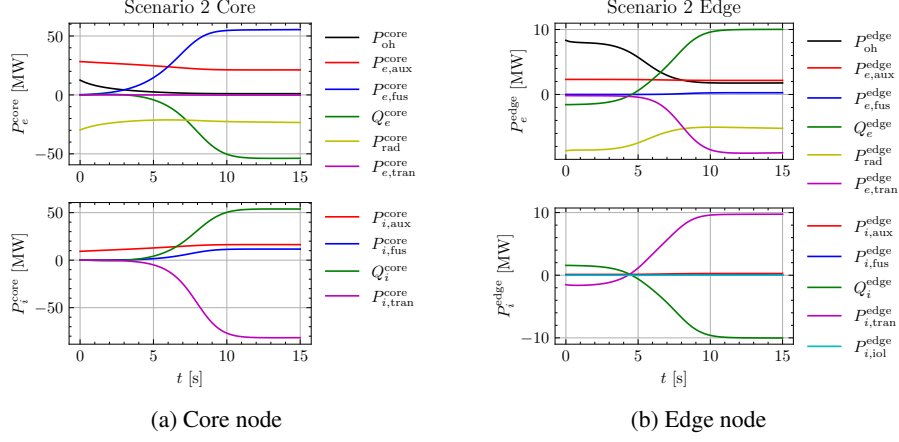


Figure 5: Powers of ITER inductive operation scenario 2.

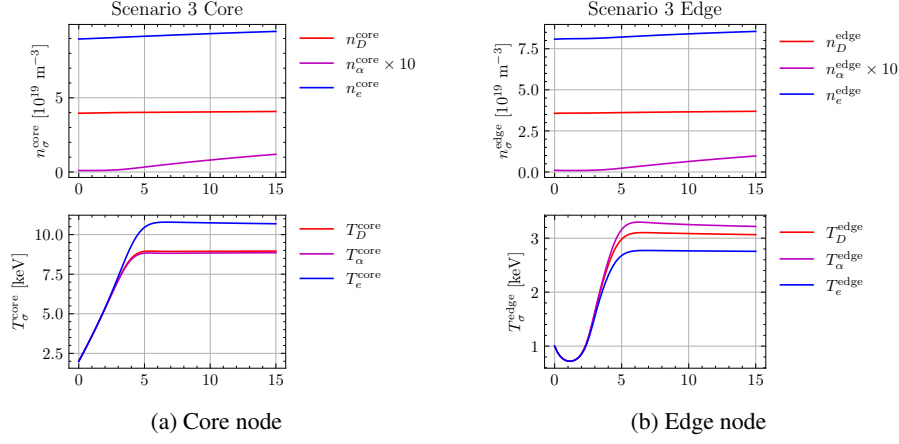


Figure 6: Densities and temperatures of ITER hybrid operation scenario 3.

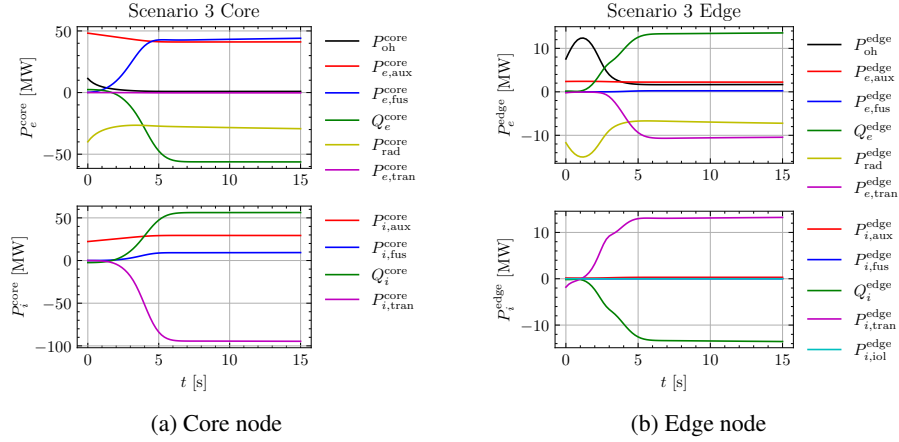


Figure 7: Powers of ITER hybrid operation scenario 3.

lower than in the inductive one, but the safety factor at the 95% flux surface is higher. Additionally, the plasma current is roughly equally divided between current drive and bootstrap current. The simulation results for the non-inductive scenario 4 are presented in Figures 8 and 9. The ion and electron temperatures reach a steady state at around 12 s. Compared to inductive scenario 2, non-inductive scenario 4 exhibits higher fusion and auxiliary heating. Additionally, the energy transported

from core electrons to the edge is significantly greater. However, Coulomb collisional energy transfer occurs from ions to electrons since the core electron temperature is lower than the core ion temperature. No energy excursion due to fusion alpha heating is observed in this simulation.

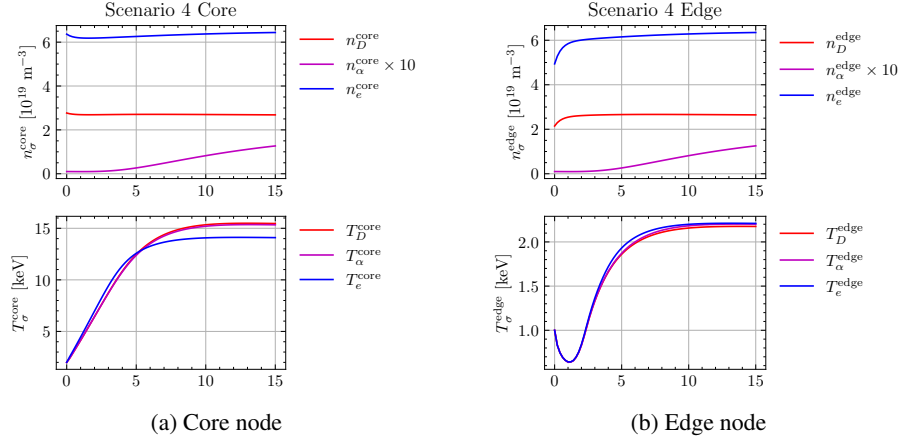


Figure 8: Densities and temperatures of ITER non-inductive operation scenario 4.

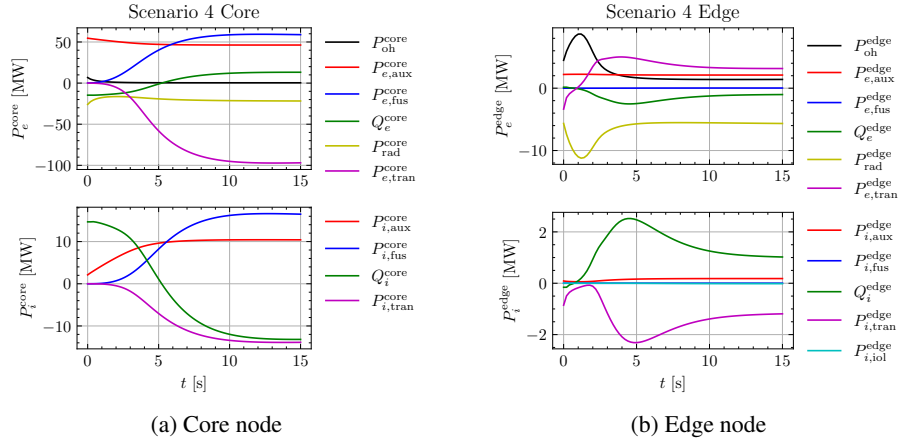


Figure 9: Powers of ITER non-inductive operation scenario 4.